Canadian Journal of Chemistry

Published by
THE NATIONAL RESEARCH COUNCIL OF CANADA

Journal canadien de chimie

Publié par
LE CONSEIL NATIONAL DE RECHERCHES DU CANADA

Volume 55 Number 11 June 1, 1977

Volume 55 numéro 11 1 juin 1977

Effects of phase density on ionization processes and electron localization in fluids

JOSHUA JORTNER
Department of Chemistry, Tel-Aviv University, Tel-Aviv, Israel

AND

ARIEL GAATHON[1]
Department of Physical Chemistry, The Hebrew University, Jerusalem, Israel

Received November 1, 1976

JOSHUA JORTNER and ARIEL GAATHON. Can. J. Chem. **55**, 1801 (1977).

In this paper we shall be concerned with the energetics of selective ionization processes in simple nonpolar fluids and with the nature of electron localization in polar fluids, studied over a wide density range. The static features of bound Wannier states and of the conduction band in simple solid and fluid insulators were monitored by vacuum-ultraviolet absorption spectroscopy and photoemission studies providing quantitative information concerning the energy of the bottom of the conduction band, impurity ionization potentials, and adiabatic polarization energies. Electron localization in subcritical and supercritical water and ammonia was studied by pulse radiolysis methods. A critical, temperature dependent, density ρ_C for electron localization in ND_3 was observed. The weak density dependence of the maximum of the absorption band of the localized electron in D_2O and ND_3, and the temperature and density dependence of ρ_C in ND_3, provide compelling evidence for the crucial role of density fluctuations on electron localization in polar fluids.

JOSHUA JORTNER et ARIEL GAATHON. Can. J. Chem. **55**, 1801 (1977).

Dans cette publication on est intéressé à l'énergie des processus d'ionisation sélective dans des fluides non-polaires simples et avec la nature de la localisation électronique dans des fluides polaires qui sont étudiés sur un grand écart de densité. On a déterminé les caractéristiques statiques des états Wannier liés et des bandes de conduction dans des solides simples et dans des isolants fluides en faisant appel à la spectroscopie d'absorption dans l'ultra-violet lointain et par des études de photoémission fournissant des informations quantitatives concernant l'énergie au minimum de la bande de conduction, les potentiels d'ionisation des impuretés et les énergies de polarisation adiabatique. On a étudié, par des méthodes de radiolyse pulsées, la localisation d'électrons dans de l'eau et de l'ammoniac à l'état sous-critique et supercritique. On a observé une densité critique, ρ_C, dépendant de la température, pour la localisation d'électrons dans ND_3. La faible dépendance sur la densité du maximum de la bande d'absorption des électrons localisés dans D_2O et ND_3 et les dépendances sur la température et la densité de ρ_C dans ND_3 fournissent des implications importantes sur le rôle crucial des fluctuations de densité sur la localisation des électrons dans des fluides polaires.

[Traduit par le journal]

I. Introduction

The understanding of the nature of excess electron states in fluids (1–3) provides a challenging problem in the general area of the physics and chemistry of disordered materials. In the past decade there has been substantial experimental and theoretical progress in the elucidation of the electronic structure and of electron transport in polar and in nonpolar

---

[1] Present address: Department of Biological Sciences, Columbia University, New York, NY, U.S.A.

liquids with regard to the molecular composition, the static structure, and the dynamic properties of the medium. An attempt to provide a general classification of excess electron states in fluids is presented in Table 1. The gross features of the quasi-free electron state (3–5) (class 1) as well as localized excess electron states resulting from bubble formation in nonpolar fluids (3–5) (class 5) and via the formation of the solvated electron in polar fluids (1, 2; for a recent review, see ref. 6) (class 6) are well understood. On the other hand, the nature of 'intermediate type' excess electron states with regard to temporal (time-resolved) and structural aspects of electron localization are not yet well established. These include 'quasi-localized' states (class 2) originating from fluctuations in the local electron–medium potential which may result in Anderson localization (3, 7) of the excess electron, self-trapping by small configurational fluctuations (8) (class 3), and electron localization by pre-existing traps (9–11) (class 4). The present paper will be concerned with physical information concerning:

(*1*) The energetics of ionization processes and the features of the quasi-free excess electron states in simple nonpolar solids and fluids. Spectroscopic techniques, utilizing vacuum-ultraviolet optical absorption spectroscopy and electron photoemission to probe energy levels, were applied to these problems.

(*2*) Electron localization in polar fluids, studied by monitoring the yields of localized excess electrons. Conventional time-resolved absorption spectroscopy combined with pulse radiolysis methods for determination of the yields of localized electrons were utilized.

While most of previous studies of excess electron states in fluids focused attention on electrons in liquids, the results of the work reported herein will provide pertinent information regarding the effects of phase density on ionization processes and on electron localization, studied over a broad density range.

II. Selective Ionization Processes in Solids and in Dense Fluids

The optical absorption spectra of pure and of lightly doped simple insulators, such as solid and liquid rare gases, can be analyzed in terms of stable exciton or impurity states converging to the bottom of the conduction band (13, 15; for a recent review see ref. 12). The relative simplicity of these exciton and impurity states makes it possible to gain detailed information regarding ionization processes in a dense medium. The sources of experimental information regarding such selective ionization processes are:

(*A*) Identification of Wannier bound states in pure materials and of Wannier atomic or molecular impurity states in doped insulators by absorption spectroscopy. The Wannier series converges to the bottom of the conduction band.

(*B*) From the convergence limit of the Wannier series studied by absorption spectroscopy one can obtain the band gap, E_G, in the pure substance or the impurity ionization potential, $E_G{}^i$, of the impurity in the medium.

(*C*) The energetics of the Wannier states, monitored by absorption spectroscopy, result in basic information regarding the characteristics of the conduction band. In particular, from the effective Rydberg constant of the Wannier series one can deduce the effective mass of the electron near the minimum of the conduction band.

(*D*) The threshold for photoconductivity in the pure solid or liquid results in a direct measurement of E_G, while the photoconductivity threshold $E_G{}^i$ of the doped insulator yields the ionization potential of the impurity in the medium.

(*E*) The threshold for external photoemission from the pure material, E_{TH}, or from the doped insulator, $E_{TH}{}^i$, results in the external ionization potentials. From the combination of optical spectra and photoemission yields in pure or in doped insulators one can determine the energy V_0 of the bottom of the conduction band relative to the vacuum level.

In what follows we shall consider first the energetics of ionization processes in solids where Wannier series are now well documented. Subsequently, we shall consider the application and implication of these results for fluids over a wide density range.

In pure insulators low-lying stable excitons originate from Bloch states near the top of the valence band and in the vicinity of the bottom of the conduction band (16–18). Impurity excited states below interband threshold can be considered in terms of a hole in the energetically flat impurity band correlated with electron states, which are constructed from levels near

TABLE 1. Excess electrons in fluids*

Definition	Physical state of fluid	Nature of electron–fluid interaction	State of excess electron	Time scale	Characteristic systems and physical properties
1. Quasi-free	Structure of fluid unperturbed	Single scattering by fluid structure factor $s(Q)$ Multiple scattering off density fluctuations (?)	Extended	Adiabatic injection in *all* fluids Long t scale when $V_0 < E_t^B$	$\mu \geq 10^2$ V^{-1} cm^2 s^{-1} All fluids short time Heavy rare gases Ar, Kr, Xe Low density nonpolar (He) and polar (H_2O, NH_3) fluids
2. Quasi-localized	Structure of fluid unperturbed	Strongly changing local potentials	Localized (Anderson model) (?) or extended	Long t scale	$0.1 \leq \mu \leq 10$ V^{-1} cm^2 s^{-1} T activated motion Some hydrocarbons (?) Transition range in He gas (?)
3. Self-trapped by small density and/or structural fluctuations	Small configurational fluctuations induced by e	Local attractive potential (homopolaron)	Localized (?)	$t \geq \tau_{MM}$	$0.1 \leq \mu \leq 10$ V^{-1} cm^2 s^{-1} T activated Some hydrocarbons (?)
4. Localized by pre-existing 'traps'	Unperturbed pre-existing configurational fluctuations	Local attractive potential of 'trap'	Localized	$t \sim \sigma\langle v\rangle n_{trap}$ $t \leq \tau_{DR}$	$\mu \leq 0.1$ cm^2 V^{-1} s^{-1} Polar liquids 'short' times $\tau_{DR} \sim 10^{-10}$–10^{-12} s Polar molecular clusters in hydrocarbons. Polar gases
5. Localized by bubble formation	Formation of microscopic cavity, large configurational changes	Essentially repulsive $V_0 > E_t^B$	Localized	$t \gg \tau_{MM}$	$\mu \sim 10^{-2}$–10^{-3} cm^2 V^{-1} s^{-1} Volume expansion Optical spectra Liquid He, Ne
6. Localized by large local configurational changes	Radial and orientational changes induced by e	Bound polaron in polar liquids	Localized	$t \gtrsim \tau_{DR}$	$\mu \sim 10^{-3}$ cm^2 V^{-1} s^{-1} Optical spectra, etc. solvated electron in polar liquids

*V_0 = Energy of quasi-free electron (qfe) state; μ = electron mobility; σ = cross section for trapping of qfe by a pre-existing cluster; E_t^B = energy of ground state energy of localized electron (class 5 or 6) in the same fluid; τ_{MM} = time scale for molecular motion; τ_{DR} = dielectric relaxation time.

the bottom of the conduction band. In insulators such as solid rare gases, we are primarily concerned with deep exciton and impurity states, where pseudopotential theory was invoked to rationalize the observation of Wannier states (18). Such highly excited deep exciton and impurity states can be described in terms of the effective mass equation (18, 19). If the edges of both valence and conduction band occur at some point $\boldsymbol{k}_0$ in the Brillouin zone (BZ) and the interband transition is dipole allowed, one is concerned with direct excitons. For impurity excitations $\boldsymbol{k}_0$ corresponding to the minimum of the conduction band and direct impurity excitations are always encountered. In simple insulators $\boldsymbol{k}_0$ correspond to the Γ point in the BZ. The high exciton levels E_n and impurity levels $E_n{}^{\mathrm{i}}$ (see Figs. 1 and 2) are described in terms of a hydrogenic series converging to the bottom of the conduction band,

$$[1] \qquad E_n = E_{\mathrm{G}} - G/n^2$$

$$[2] \qquad E_n{}^{\mathrm{i}} = E_{\mathrm{G}}{}^{\mathrm{i}} - G^{\mathrm{i}}/n^2$$

where E_{G} corresponds to the interband gap at $\boldsymbol{k}_0$ while $E_{\mathrm{G}}{}^{\mathrm{i}}$ is the impurity energy gap (see Figs. 1 and 2). The latter energetic quantity, which in the chemist's language just corresponds to the ionization potential of the impurity in the solid, is given by

$$[3] \qquad E_{\mathrm{G}}{}^{\mathrm{i}} = I_{\mathrm{g}} + P_+ + V_0$$

where I_{g} is the impurity gas phase ionization potential, P_+ is the (adiabatic) medium polarization energy by the impurity positive ion, and V_0 designates the energy of the bottom of the conduction band relative to the vacuum level. G and G^{i} in [1] and [2] correspond to the effective Rydberg constants for the exciton and for the impurity hydrogenic series, respectively, which are given by

$$[4] \qquad G = 13.6(\mu/\varepsilon^2)\ \mathrm{eV}$$

$$[5] \qquad G^{\mathrm{i}} = 13.6(m^*/\varepsilon^2)\ \mathrm{eV}$$

$$[6] \qquad \mu = m^* m_{\mathrm{h}}/(m^* + m_{\mathrm{h}})$$

where m^* is the electron effective mass near the bottom of the conduction band, m_{h} is the hole effective mass, again near $\boldsymbol{k}_0$, while ε is the static dielectric constant of the solid. In view of the large value of m_{h} we expect that G is close to G^{i}.

High exciton and impurity states, characterized by the quantum number $n \geq 2$, do not reveal any relation to the atomic or molecular excited states of the constituents in the gas phase, and should be viewed as one-electron excitations of the dense medium below the direct interband threshold. Relevant examples for Wannier exciton states in pure rare-gas solids are presented in Figs. 3 and 4. Focusing attention on Wannier impurity states the following quantitative information concerning the static properties of the conduction band emerges.

(*1*) From the effective Rydberg constant G^{i}, [5], together with the static dielectric constant, one can deduce m^*. These values are invariant

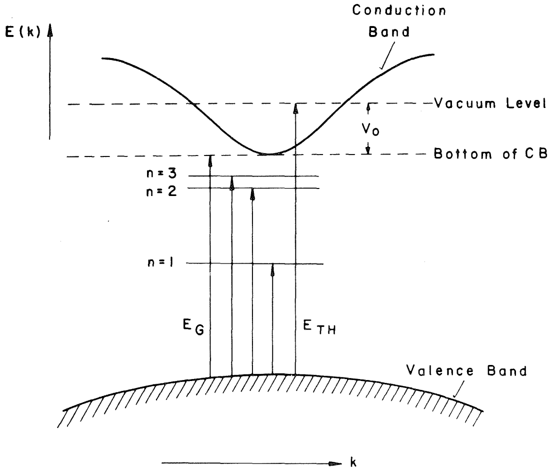

FIG. 1. A schematic representation of the energy levels of a simple pure insulator.

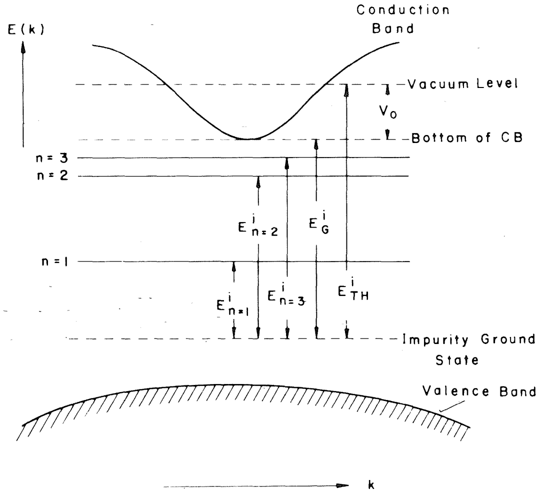

FIG. 2. A schematic representation of the energy levels of Wannier impurity states in an insulator.

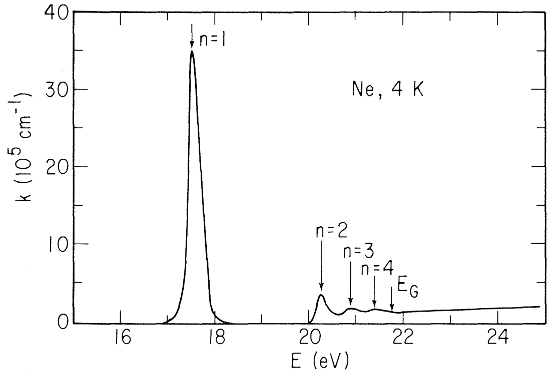

FIG. 3. The absorption spectrum of solid Ne (15, 29).

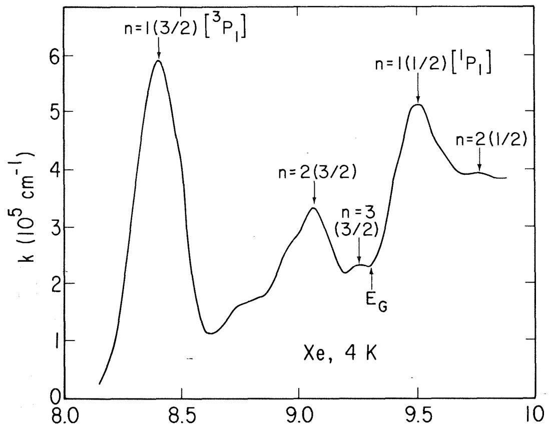

FIG. 4. The absorption spectrum of solid Xe (55).

with respect to the nature of the particular impurity.

(*2*) The convergence limit of the impurity Wannier series results in $E_G{}^i$, the impurity ionization potential in the insulator.

(*3*) A direct and reliable approach to derive V_0 rests on the combination of spectroscopic data for $E_G{}^i$ with photoemission yield data from lightly doped insulators. The photoemission threshold, $E_{TH}{}^i$, is

$$[7] \qquad E_{TH}{}^i = I_g{}^i + P_+$$

whereupon from [3] and [7] we obtain

$$[8] \qquad V_0 = E_G{}^i - E_{TH}{}^i$$

An analogous relation of the form

$$[9] \qquad V_0 = E_G - E_{TH}$$

holds for the pure solid and liquid insulator.

III. Wannier-type Impurity States in Solid Insulators

We now turn to a brief survey on Wannier impurity states in simple solids. The best known example involves dilute rare-gas alloys (20–22, 14). Typical examples for the absorption spectra of such atomic impurity states (14) are reproduced in Fig. 5. The observation of hydrogenic Wannier impurity states is not limited to rare-gas solids and Xe impurity states were observed in other molecular crystals (23, 24) such as solid H_2, D_2, and CF_4 (Fig. 6). All these spectra pertain to large-radius atomic impurity states. Analogous molecular excitations are also amenable to experimental observation, whereupon extravalence excitations of a molecular impurity in an insulator should exhibit Wannier-type states originating from an electron wavepacket interacting with a molecular positive ion (14). The identification of such molecular excitations is complicated by congestion of vibrational structure, overlap of extravalence

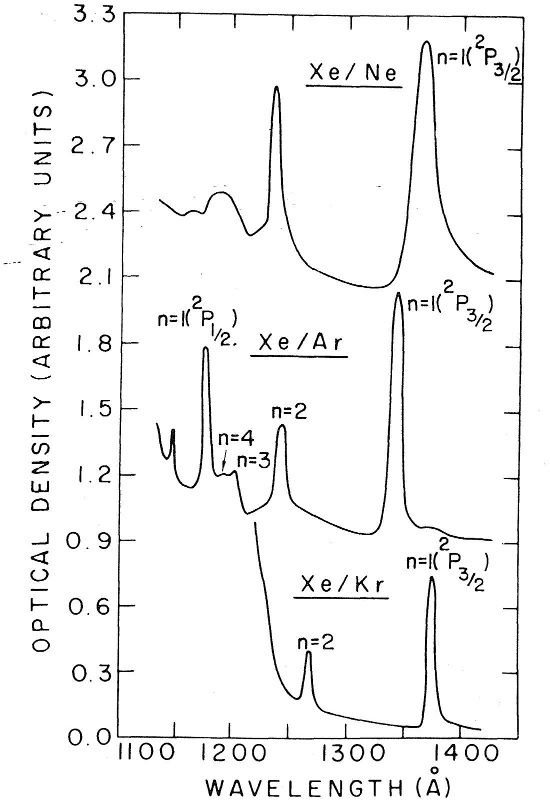

FIG. 5. The absorption spectra of dilute solid rare-gas alloys (14).

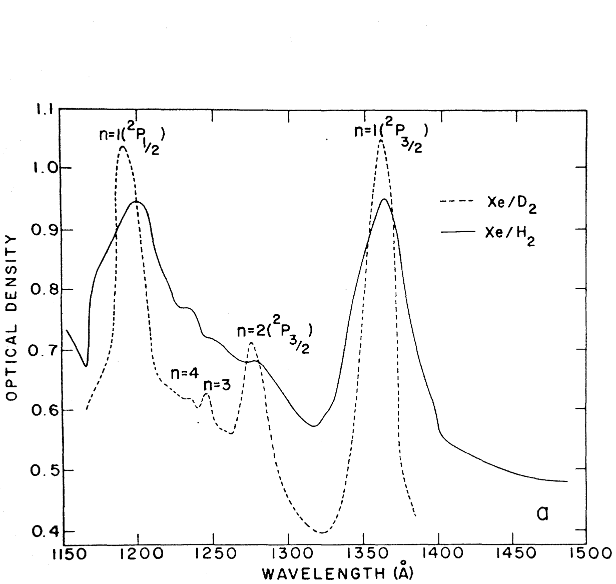

FIG. 6. Absorption spectra of Xe impurity in molecular crystals. (*a*) The absorption spectra of Xe in solid H_2 and D_2 at 6 K. (*b*) The absorption spectrum of Xe in solid CF_4 at 6 K (23).

and intravalence excitations, overlap of extravalence excitations with photodissociative continua, as well as additional line broadening originating from intramolecular electronic relaxation. A typical example for extravalence excitations of the benzene molecule (14) in rare-gas solids is presented in Fig. 7. Analysis of these data according to [2] is demonstrated in Fig. 8.

The physical information derived from solid state absorption spectroscopy is supplemented by the results of photoemission yields from pure solids and from lightly doped insulators (25–30). Figure 9 portrays the energy dependence of the photoemission yield (30) from pure Xe at 20 K. The weak peak at 1380 Å originates from extrinsic effects, while intrinsic photoemission is exhibited below ~1300 Å. Intrinsic photoemission data from atomic and molecular impurity states (26–28) (characterized by $E_{TH}{}^{i} < E_{TH}$) are presented in Figs. 10–12. Square root extrapolation of the photoemission yield *vs.* energy results in the photoemission thresholds.

In Table 2, we summarize the energetic data characterizing ionization processes in solid rare gases. The following observations are pertinent.

(*a*) $E_G{}^{i}$ is determined by the nature of the impurity state, according to [3] (see Section II).

(*b*) $E_{TH}{}^{i}$ is determined by the nature of the impurity state as is evident from [7].

(*c*) The effective Rydberg constants for impurity ionization G^i are independent of the nature of the impurity as these are determined by the host dielectric constant and by the features of the conduction band according to [5].

(*d*) The observation that $G^i \simeq G$ implies, according to [4]–[6], that $\mu \simeq m^*$, *i.e.* the hole effective mass m_h is large.

(*e*) The V_0 value derived from [8] for doped solids and from [9] for the pure solids corresponds to an intrinsic property of the solid. V_0 is identical, within experimental uncertainty, for the pure and for the doped solids and for the latter it is independent of the nature of the impurity. The self-consistency of the V_0 data provides strong evidence for the validity of the assignment of exciton and Wannier impurity states in insulators.

IV. V_0 Scale for Solid and Liquid Rare Gases

The combination of spectroscopic and photoemission data results in a reliable V_0 scale for solid rare gases. In Table 3, we compare these V_0 values with the experimental data for liquid rare gases recently determined by Tauchert (31). It is apparent that in all cases V_0 in the solid is higher than in the corresponding liquid, indicating that in the former case the contribution of short-range repulsive interactions is

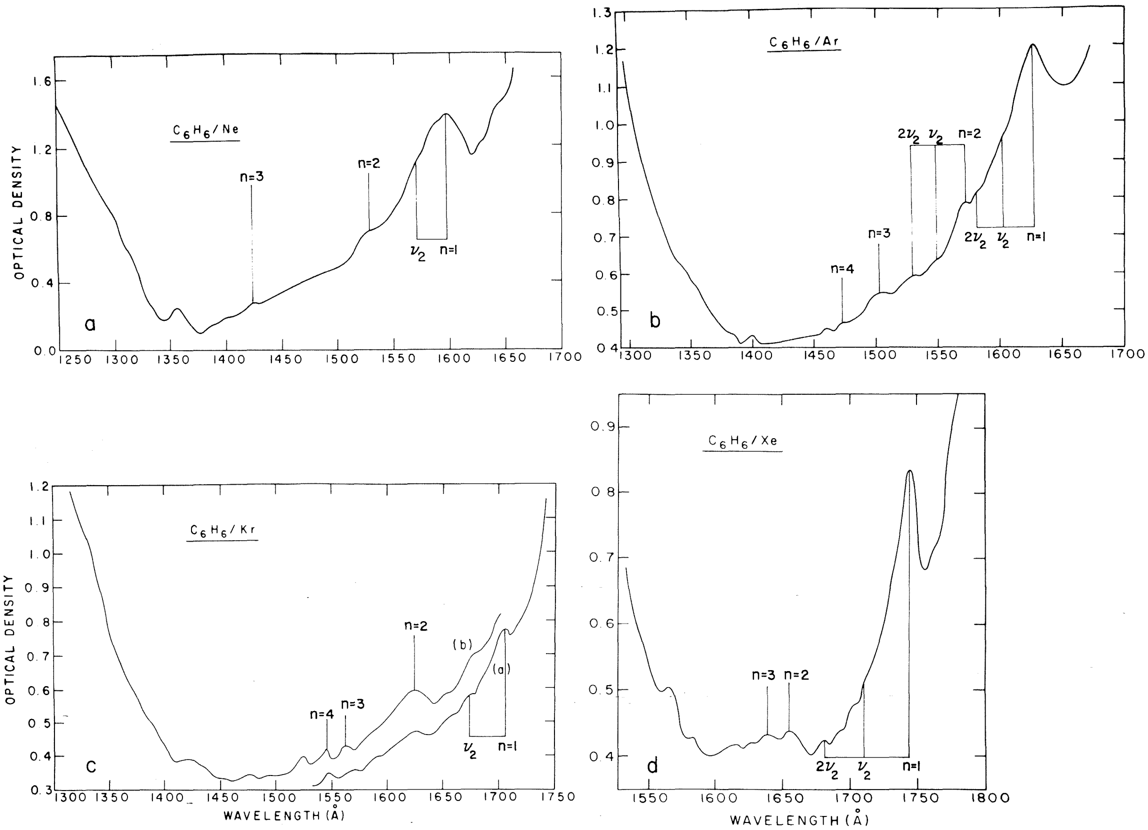

FIG. 7. Extravalence excitations of benzene in solid rare gases (14). (*a*) C_6H_6/Ne; (*b*) C_6H_6/Ar; (*c*) C_6H_6/Kr; (*d*) C_6H_6/Xe.

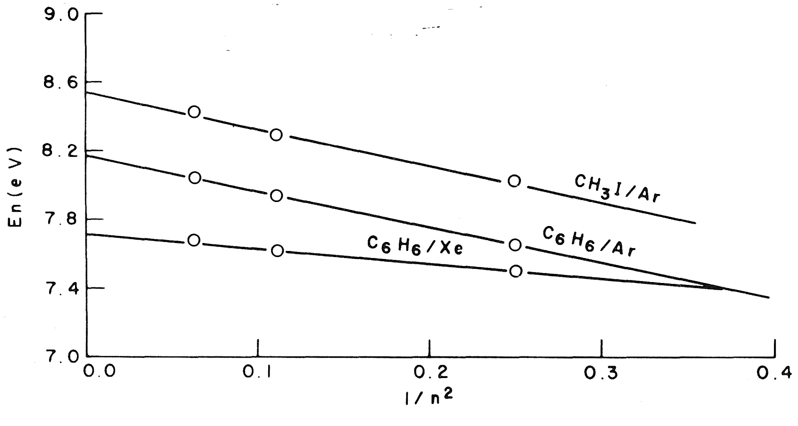

FIG. 8. Plots of E_n *vs.* $1/n^2$ for Wannier molecular impurity states in rare-gas solids.

somewhat higher. It is of interest to confront the experimental V_0 data with the prediction of the simple SJC theory (5). As is well known, the energy of the conduction band minimum for the excess electron consists of two contributions, the background polarization potential U_P and the kinetic energy term T arising from multiple scattering from nearest neighbors, so that $V_0 = T + U_P$. The SJC model provides a simple recipe for the estimate of U_P including

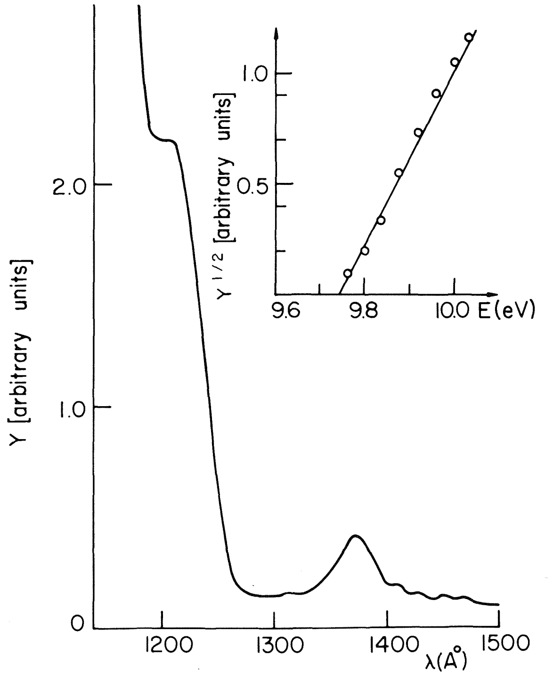

FIG. 9. Photoemission spectrum of pure Xe and 20 K (27, 30).

the screened polarization field of the surrounding atoms and for the evaluation of T by the Wigner–Seitz approximation. Table 4 summarizes the results of such calculations, where the scattering length a of the Hartree–Fock atomic field for He and Ne was taken from theoretical scattering data (5), while for Ar, Kr, and Xe, the value of a was adjusted to fit the liquid V_0 value. These semiquantitative theoretical estimates of V_0 are fraught with difficulties as Table 4 emphasizes how much smaller V_0 is than the T and the U_P terms. These theoretical estimates clearly indicate that the increase of T in the solid is somewhat higher than the corresponding decrease in U_P; however, the SJC model underestimates the relative increase of the short-range repulsive interactions in the solid as is apparent from the result for Ar. Thus this semiquantitative approach (5) should not be considered as an ultimate theory and further theoretical work in this field is required.

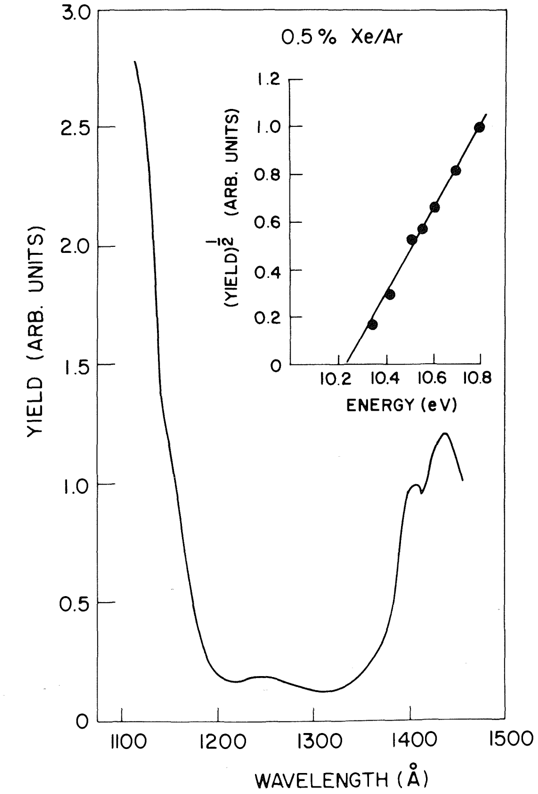

FIG. 10. Photoemission spectrum of Xe in solid Ar (28).

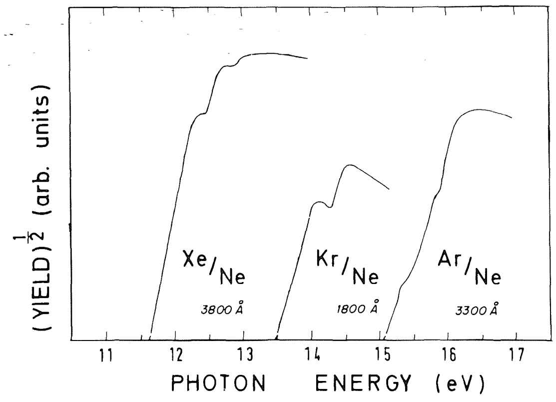

FIG. 11. Photoemission yields of atomic impurities in solid Ne (29).

V. Impurity Ionization Potentials in Solids

In Table 5 we summarize the available experimental data for the ionization potentials $E_G{}^i$ of atomic and molecular impurities in solid rare gases obtained from spectroscopic determinations of the convergence limit of Wannier impurity states. Another piece of useful energetic data involves the adiabatic polarization energy of the medium by the positive ion which can be obtained from the relation $P_+ = E_{TH}{}^i - I_g{}^i$ provided that the photoemission threshold is known or, alternatively, from [3], $P_+ = E_G{}^i -$

TABLE 2. Energetic data for pure and doped solid rare gases

System	E_G or $E_G{}^i$ (eV)	G or G^i (eV)	E_{TH} or $E_{TH}{}^i$ (eV)	V_0 (eV)
Ne (pure)	21.69	5.24	20.6	1.0 ±0.2
Ar/Ne	16.23	5.27	15.16	1.07±0.1
Kr/Ne	14.76	5.27	13.56	1.2 ±0.1
Xe/Ne	(12.63)		11.67	0.97±0.2
Ar (pure)	14.2	2.4	13.9	0.3 ±0.1
Kr/Ar	12.5		12.2	0.3 ±0.1
Xe/Ar	10.54	2.4	10.23	0.3 ±0.1
Kr (pure)	11.6		11.9	−0.3 ±0.1
Xe/Kr	10.1	1.7	10.3	−0.2 ±0.1
Xe (pure)	9.28	0.88	9.74	−0.46±0.1

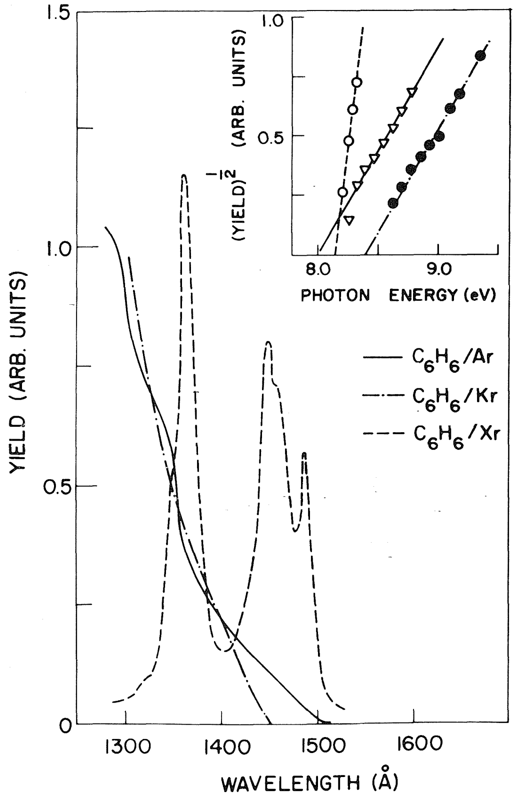

FIG. 12. Photoemission spectra of benzene in solid rare gases (28).

$I_g{}^i - V_0$ utilizing the experimental V_0 scale (Table 3). The resulting P_+ values are also given in Table 5. From these results we conclude that:

(*A*) The impurity ionization potential in the solid can exceed the gas phase ionization potential provided that V_0 is positive and large. This is the situation for atomic impurity states in solid Ne where $E_g{}^i > I_g{}^i$.

(*B*) In a solid characterized by a small positive value of V_0, such as Ar, or where $V_0 < 0$, as is the case for Kr and for Xe, we expect that $P_+ + V_0 < 0$, whereupon $E_g{}^i < I_g{}^i$.

(*C*) As $P_+ < 0$ one expects that the external photoemission threshold, [7], is always lower than the gas phase ionization potential, *i.e.* $E_{TH}{}^i < I_g{}^i$. This point was discussed by Chia and Delahay (32).

(*D*) For a given impurity in different hosts P_+ roughly increases with increasing optical dielectric constant. A rough approximation for P_+ involves the Born charging energy $P_+ \simeq (e^2/2R)(1 - (\varepsilon_{op})^{-1})$, where R is the effective radius of the impurity. It should be noted that the Born relation does not provide a quantitative account for the experimental P_+ data. Thus, for benzene in Ne, Ar, Kr, and Xe, P_+ exhibits only a weak dependence on the host matrix. Short-range repulsive interactions are of some importance as is evident from the fact that P_+ for Ar^+/Ne is lower than the corresponding values for Kr^*/Ne and for

TABLE 3. Experimental V_0 scale for solid and liquid rare gases*

System			V_0 (eV)
Liquid	^{4}He	4.2 K	+1.05
Solid	Ne	4 K	+1.1 ±0.1
Liquid	Ne	25 K	+0.67±0.05
Solid	Ar	6 K	+0.3 ±0.1
Liquid	Ar	87 K	−0.2 ±0.02
Solid	Kr	20 K	−0.25±0.1
Liquid	Kr	123 K	−0.45±0.05
Solid	Xe	40 K	−0.46±0.05
Liquid	Xe	165 K	−0.61±0.05

*Solid state data: absorption and photoemission spectroscopy (Tel-Aviv and DESY work). Liquid data: He, Sommer (53); Ar, Kekner *et al.* (54); Ne, Ar, Kr, Xe, Tauchert (31*a*).

TABLE 4. Application of the SJC theory for the calculation of V_0 in liquid and solid rare gases

System	r_s (Å)	α (Å^3)	a (Å)*	k_0 (Å^{-1})	T (eV)	U_P (eV)	V_0 (eV)	
							Calcd.	Exptl.
He(L)	2.22	0.20	0.75	0.66	1.66	−0.38	+1.28	+1.05±0.05
Ne(L)	1.86	0.39	0.56	0.71	1.91	−1.46	+0.45	+0.67±0.05
Ne(S)	1.75	0.39	0.56	0.80	2.44	−1.85	+0.60	+1.1 ±0.1
Ar(L)	2.23	1.63	0.92	0.82	2.53	−2.73	−0.20	−0.2 ±0.02
Ar(S)	2.08	1.63	0.92	0.95	3.46	−3.54	−0.08	+0.3 ±0.1
Kr(L)	2.38	2.46	1.07	0.85	2.73	−3.11	−0.38	−0.40±0.05
Kr(S)	2.21	2.46	1.07	1.00	3.84	−4.05	−0.21	−0.25±0.1
Xe(L)	2.60	4.00	1.26	0.87	2.85	−3.46	−0.61	−0.61±0.1
Xe(S)	2.40	4.00	1.26	1.04	4.12	−4.64	−0.52	−0.46±0.05

*a values for He, Ne from theoretical scattering data, for Ar, Kr, Xe chosen to fit V_0 for liquid.

TABLE 5. Ionization energies and medium polarization energies for atomic and molecular impurities in solid rare gases (all energies in eV)

Guest	Host	$E_G{}^i$	$I_g{}^i$	P_+
Ar	Ne	16.23	15.68	−0.63
Kr	Ne	14.78	13.92	−0.45
Xe	Ne	12.63	12.08	−0.48
Kr	Ar	12.50	13.92	−1.62
Xe	Ar	10.54	12.08	−1.74
Xe	Kr	10.1	12.08	−1.87
C_6H_6	Ne	(9.20)	9.24	(−1.04)
C_6H_6	Ar	8.51	9.24	−0.93
C_6H_6	Kr	8.18	9.24	−0.96
C_6H_6	Xe	7.75	9.24	−1.03
C_2H_4	Ne	10.43	10.50	−1.07
C_2H_4	Ar	9.13	10.50	−1.57
C_2H_4	Kr	8.88	10.50	−1.42
C_2H_4	Xe	8.14	10.50	−1.90
CH_3I	Ne	9.51	9.49	−0.98
CH_3I	Ar	8.58	9.49	−1.11
CH_3I	Kr	8.13	9.49	−1.16
CH_3I	Xe	—	9.49	—

Xe*/Ne, while P_+ for the latter two systems is practically identical.

VI. Excitons in Fluids

While one-electron excitations in crystalline insulators are quite well understood, the nature of analogous excitations in fluids is not yet elucidated. It was suggested (33) that large-radius Wannier-type exciton states are amenable to experimental observation in a dense fluid where electron–medium interaction is sufficiently weak. Liquid rare gases provide suitable candidates for the search for such electronic excitations which are of considerable interest in relation to general problems of electronic states in disordered materials as well as in the context of deriving quantitative information concerning ionization processes in simple liquids. From the experimental point of view evidence has been reported (34, 35) for the identification of the $n = 2$ exciton in liquid Xe and the $n = 2$ impurity state of Xe in liquid Ar (36). In order to establish the nature of Wannier states in dense simple fluids it will be interesting to obtain a continuous description of the electronic excitations of a guest atom or molecule in a host fluid where the fluid density is varied over a broad density range. One has to distinguish carefully between intravalence excitations, low extravalence impurity excitation, and high extravalence impurity excitations, all of which are exhibited at low and intermediate densities of the host medium, and sort out the large Wannier states which may appear in the high density fluids. The general characteristics of different types of impurity excitations in a host fluid are summarized in Table 6.

Messing (37) has recently studied the absorption spectra of atomic and molecular impurity states in simple dense fluids over a wide density range. The absorption spectra of the Xe/Ar system from the atomic limit up to the solid one is presented in Figs. 13 and 14. At low and at moderate Ar densities ($\rho = 0$–0.6 g cm^{-3}) five 'atomic' excitations are exhibited (Fig. 13) in the range 1150–1300 Å.

(I) $6s'$ [1/2] $J = 1$ located in the atomic limit at 1296 Å.

(II) $5d$ [1/2] $J = 1$ located in the atomic limit at 1250 Å.

(III) $5d$ [5/2] $J = 3$ which is symmetry forbidden in the isolated atom, being pressure induced around 1210 Å.

(IV) $5d$ [3/2] $J = 1$ located at 1192 Å in the atomic limit.

TABLE 6. Medium effects on absorption spectra of a guest atom in a host fluid and solid*

	Guest atomic states		
States of perturbing medium	(*1*) Intravalence excitations	(*2*) Lowest extravalence $\Delta n_A = 1$ excitations	(*3*) High extravalence $\Delta n_A \geq 2$ excitations
(*A*) Spectral perturbations by a foreign gas at low and at moderate densities	(*a*) Spectral shifts (small red or blue) and line broadening (*b*) Appearance of 'red' or 'blue' satellites (*c*) Symmetry breaking, induction of forbidden transitions	(*a*) Shifts (red at low densities, blue at higher densities) and line broadening (*b*) Appearance of 'red' or of 'blue' satellites (*c*) Symmetry breaking, induction of forbidden transitions	(*a*) Spectral shifts (red or blue) (*b*) States converges into (perturbed) ionization potential
(*B*) Spectral effects of high density fluid or liquid	Same as *1A*	(*a*) Large spectral shifts (blue) (*b*) Satellites disappear, merge with main line into a broad band (*c*) Forbidden transitions exhibited	(*a*) States 'disappear' (*b*) Appearance of high Wannier $n \geq 2$ states (*c*) Wannier states converge into bottom of conduction band
(*C*) Spectral effects in a solid	(*a*), (*b*), (*c*) same as *1A* (*d*) Crystal field splitting of degenerate excited states	Same as *2B*	Same as *3B* Wannier states well resolved due to line narrowing relative to liquid

*n_A, atomic or molecular one-electron quantum number (qn); n, qn for Wannier states.

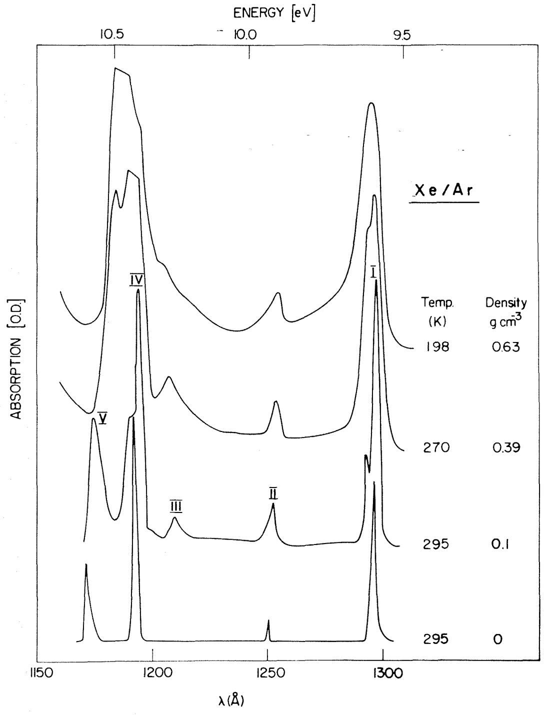

FIG. 13. The absorption spectra of Xe in fluid Ar at low densities (37).

(V) 7*s* [3/2] $J = 1$ located at 1170 Å in the atomic limit.

In the high Ar density region (Fig. 14) the absorption band in the range 1225–1250 Å exhibits an appreciable enhancement for $\rho > 0.8$ g cm^{-3}. In Fig. 15 we present Messing's results for the intensity ratio of this absorption relative to the intensity of transition I. The intensity enhancement of the 1225–1250 Å band in the Xe/Ar system is entirely different from the behavior of the Xe/Ne system where this intensity ratio reveals only a weak density dependence. Messing (37) assigned the strong absorption band located around 1250 Å in the Xe/Ar system of high Ar densities $\rho > 0.8$ g cm^{-3} to the $n = 2$ Wannier impurity states in fluid Ar. Making use of [3] one can then provide an estimate for the Xe impurity ionization potential in liquid Ar assuming that the electron effective mass m^* in the liquid is equal to that in the solid. We then obtain $E_G{}^i = 10.9$ eV for Xe in liquid Ar and $P_+ = 1.0 \pm 0.2$ eV for the polarization energy of the liquid.

It is of considerable interest to obtain information regarding the density dependence of the ionization potential of an impurity in a

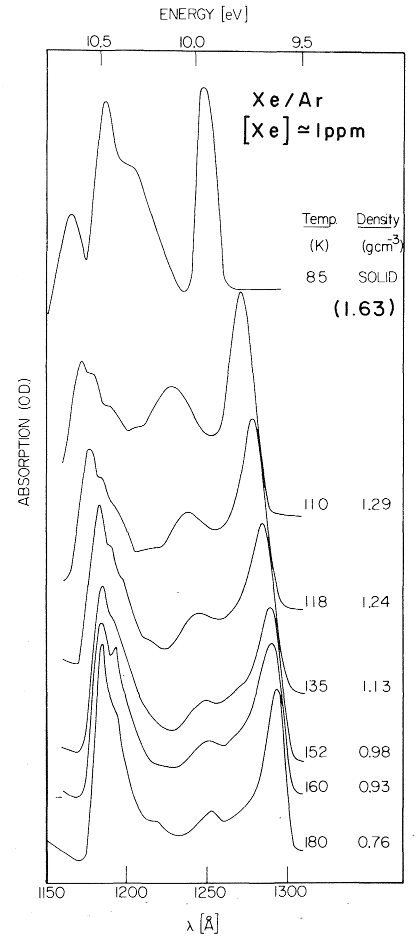

FIG. 14. The absorption spectra of Xe in fluid Ar at high Ar densities (37).

fluid. Messing (37) has studied the vacuum-ultraviolet spectra of CH_3I in Ar over a broad density range. At low densities six Rydberg series are exhibited, three of which converge to the first ionization potential (38). In the Ar density range $\rho = 0$–$0.5\ g\ cm^{-3}$ five members $n = 1$–5 of the Rydberg series could be clearly observed (37). Analysis of these data using the isolated molecule quantum defects (38) results in $G^i = 9.6\ eV$ and $E^i = 9.2\ eV$ for CH_3I at $\rho = 0.34\ g\ cm^{-3}$. In Table 7 we summarize the available experimental information derived from spectroscopic data concerning atomic and ionization potentials in fluids (37). These results demonstrate the gradual decrease of the impurity ionization potential with increasing fluid density. Such a pattern will be exhibited in any fluid where $V_0 < 0$ as is the case for Ar. It is also worthwhile to note that P_+ in the liquid is considerably lower than in the solid, a difference which cannot be reconciled just by the 15% change in the dielectric constant. Obviously, these interesting areas of electronic excitations and ionization processes in fluids deserve further experimental and theoretical effort.

Up to this point we have been concerned with some of the intrinsic features of one-electron excitations in solid and liquid insulators which provide information concerning the energetics of ionization processes in fluids and some static characteristics of the conduction band in such systems. We shall now proceed to discuss some dynamic aspects of electron localization in dense fluids.

VII. Electron Localization in Polar Fluids

Excess electrons in He gas at low temperatures undergo a sharp 'transition' from the quasi-free state to a localized bubble state with increasing density (3, 39–41). Levine and Sanders (39) have demonstrated that the mobility of electrons injected into He gas exhibits a dramatic drop of some four orders of magnitude over a density range of ~10%. The nature of the electronic states and electron transport in the transition region were described in terms of the Anderson model (3) by the percolation picture (42) and by a phenomenological model where extended and localized states coexist (43, 44). Electron localization in subcritical and in supercritical polar fluids at sufficiently high densities is expected to be a general phenomenon, while at low densities of a polar fluid the quasi-free excess electron state will be energetically stable. One thus expects that in a polar fluid, as in the case of He, a 'transition' from the localized state to the quasi-free state will be exhibited with decreasing fluid density (45). The problem of electron localization in polar fluids as a function of density (and other thermodynamic variables of state) is of considerable interest (45–49). The following questions are relevant in this context.

(*1*) Can one observe a 'critical' density, ρ_C, for the 'transition' between localized and quasi-free excess electron states in a polar fluid?

(*2*) What are the physical properties of the localized excess electron in a polar fluid over a broad density range where the localized state is thermodynamically stable?

Points *1* and *2* require basic experimental

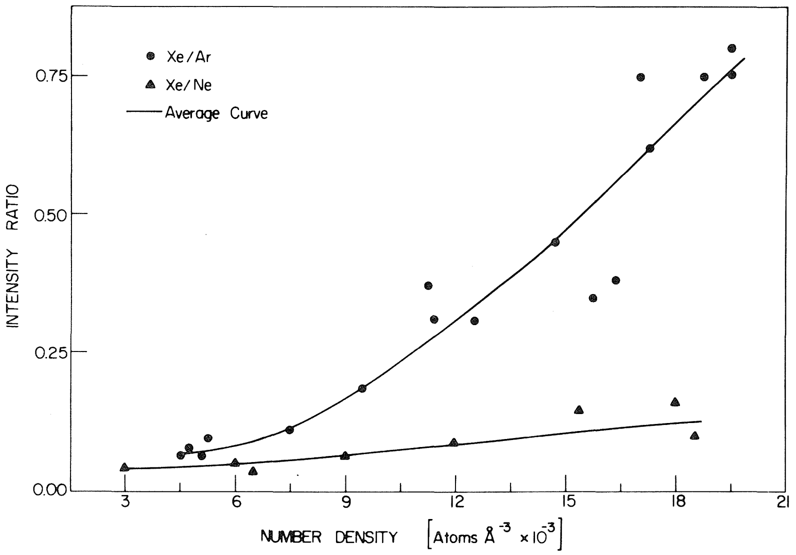

FIG. 15. The density dependence of the intensity ratio of the 1250 Å absorption to the $^1S_0 \rightarrow {}^1P_1$ transition (band I) in Xe/Ar and in Xe/Ne (37).

TABLE 7. Ionization potentials of some atomic and molecular impurities in fluid Ar (from ref. 37*a*) (solid state data are given for comparison)

Guest	Host	$E_G{}^i$ (eV)	$I_g{}^i$ (eV)	G (eV)	$P_+ + V_0$ (eV)	P_+ (eV)
Xe	Liquid $\rho = 1.35\ \mathrm{g\ cm^{-3}}$	10.9	12.13	(3.0)	−1.23	−1.03
Xe	Solid $\rho = 1.7\ \mathrm{g\ cm^{-3}}$	10.54	12.13	2.4	−1.59	−1.79
CH_3I	Supercritical $\rho = 0.34\ \mathrm{g\ cm^{-3}}$	9.2	9.55	9.6	−0.35	—
CH_3I	Liquid $\rho = 1.35\ \mathrm{g\ cm^{-3}}$	8.7	9.55	(3.0)	−0.85	−0.65
CH_3I	Solid $\rho = 1.7\ \mathrm{g\ cm^{-3}}$	8.6	9.55	2.3	−0.95	−1.15
CH_2O	Liquid $\rho = 1.24\ \mathrm{g\ cm^{-3}}$	10.2	10.88	3.8	−0.68	—

information. Supplementary theoretical work should be directed towards the elucidation of the following problems.

(*3*) The electron localization process in polar fluids with respect to the role of configurational fluctuations, pre-existing traps, etc.

(*4*) A proper theoretical description of localized excess electron states with regard to the role of short-range and long-range interactions.

A theoretical study of the properties of localized excess electrons and of their thermodynamic stability in a *homogeneous* polar fluid was conducted by Gaathon and co-workers (48, 49). He considered the molecular model for the localized excess electron incorporating short-range attractive and repulsive interactions with the first 'molecular' coordination layer, which consists of N molecules, and long-range polarization interactions with a medium characterized by the mean fluid density beyond the first coordination layer. This homogeneous model results in the following predictions.

(*a*) The critical densities for electron localization in H_2O and NH_3 (Table 8) are obtained from a modified energetic stability criterion which incorporates entropy changes accompanying the formation of the first coordination layer.

(*b*) The density dependence of the absorption band maximum $h\nu_{max}$ exhibits three distinct regions. (b.1) At high densities ($\rho = 1.2$–$1.0\ g\ cm^{-3}$ for H_2O) $h\nu_{max}$ drops fast with decreasing ρ. (b.2) Over a broad density range ($\rho = 1.0$–$0.1\ g\ cm^{-3}$ for H_2O) $h\nu_{max}$ exhibits a weak ρ dependence. (b.3) At lower densities ($\rho < 0.1\ g\ cm^{-3}$ in H_2O) $h\nu_{max}$ decreases fast with decreasing ρ.

Experimental studies of the absorption spectra and the yields of localized excess electrons in subcritical and supercritical water and ammonia were conducted by Schindewolf and co-workers (46, 47) and by Gaathon (45, 48, 49). Extensive experimental data for electron localization in D_2O, NH_3, and ND_3 were obtained (49) in the density range $\rho = 1.0$–$8 \times 10^{-3}\ g\ cm^{-3}$ ($p = 1$–400 atm, $T = 273$–670 K) for D_2O and $\rho = 0.6$–$10^{-2}\ g\ cm^{-3}$ ($p = 1$–200 atm, $T = 273$–430 K) for NH_3 and ND_3. Pulse radiolysis techniques were employed.

Figures 16 and 17 portray typical absorption spectra (49) of localized electrons in subcritical and supercritical D_2O. The experimental density dependence of $h\nu_{max}$ (corrected for temperature effects) is presented in Fig. 18. In this figure these experimental results are confirmed with the theoretical predictions (Section *b*). We note that the experimental density dependence in region b.1, where a sharp drop of $h\nu_{max}$ is predicted, and in range b.2, where $h\nu_{max}$ exhibits a weak density dependence, is in reasonable agreement with the trend predicted by the homogeneous model. However, in the low density range $\rho < 10^{-1}\ g\ cm^{-3}$ the experimental values of $h\nu_{max}$ are practically independent of the fluid density in marked contrast to the expectations based on the homogeneous model which envisions a fast drop of $h\nu_{max}$ with decreasing density in range b.3.

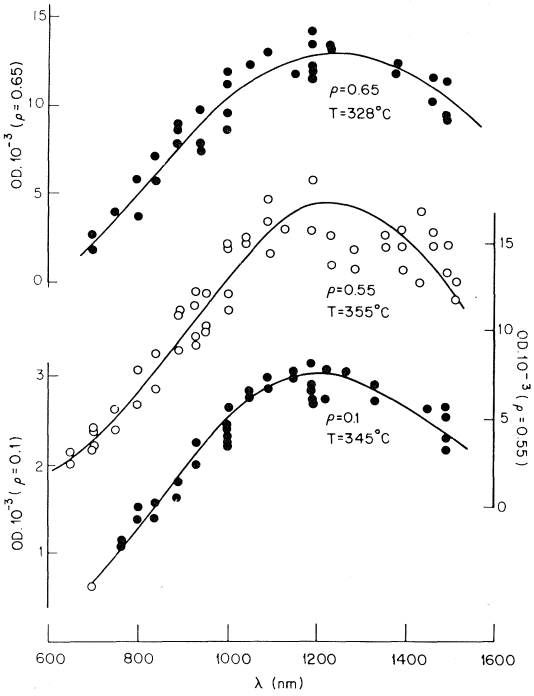

FIG. 16. The absorption spectra of the localized electron in subcritical D_2O (49).

The yields for the formation of localized excess electron states in D_2O and in ND_3 were determined by two independent methods (49). First, time-resolved absorption of the localized electron was found to obey second order decay kinetics and extrapolation of these results to $t = 0$ resulted in the yield. Second, the absorption of the localized electron was monitored during electron pulses of the duration of $\tau = 0.3\ \mu s$ and $\tau = 1.5\ \mu s$, the data being analysed according to the relation $d[e_l]/dt = \alpha\rho I - k[e_l]^2$ where α is the yield of the localized electrons, I is the intensity of the electron beam, ρ is the fluid density, and k is the bimolecular recombination rate constant. The experimental procedures for the determination of the yields of the localized electron provide proper corrections for the 'kinetic instability' of the localized state, originating from efficient recombination, and result in reliable experimental data for the initial yields. The density and temperature dependence of the yields α in D_2O and in ND_3 are displayed in Figs. 19 and 20. From these results we conclude that:

(*1*) In D_2O the localized excess electron state is stable throughout the entire density range $8 \times 10^{-3}\ g\ cm^{-3} < \rho < 1.0\ g\ cm^{-3}$ and up to $T = 673$ K. Thus in supercritical D_2O $\rho_C < 8 \times 10^{-3}\ g\ cm^{-3}$. This experimental result is in conflict with the theoretical prediction of the homogeneous model (Table 8).

(*2*) Electron localization in ND_3 (Fig. 20) exhibits a more complex and more interesting behavior. Near the liquid–vapor coexistence curve (CEC) electron localization is observed up to the lowest density $\rho \simeq 5 \times 10^{-3}\ g\ cm^{-3}$

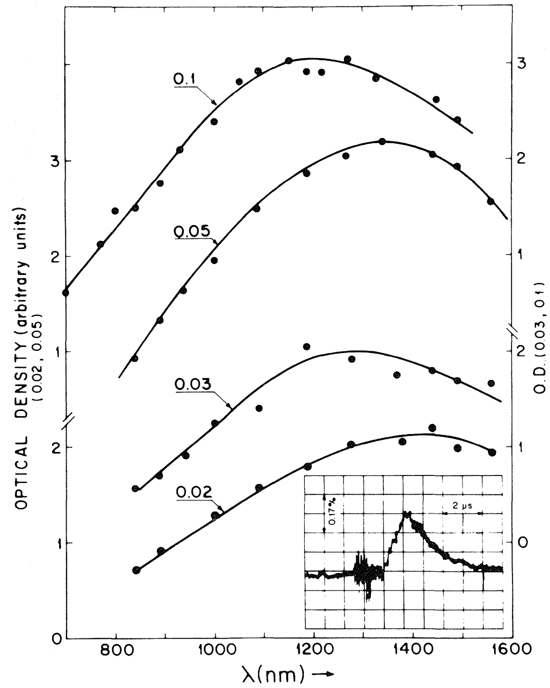

FIG. 17. Absorption spectra of the localized electron in D_2O vapor. The vapor densities (relative to the liquid at 4°C) are indicated by the numbers above the curves (48, 49). (Reprinted with permission from the Journal of Chemical Physics, **58**, 2648 (1973). Copyright by the American Institute of Physics.)

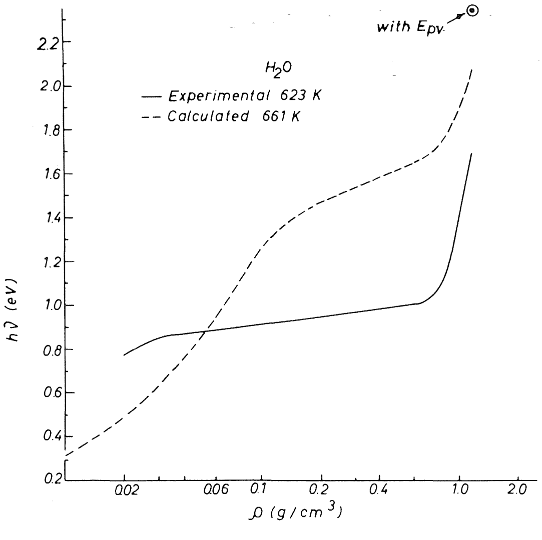

FIG. 18. The density dependence of the band maximum of the localized electron in D_2O (49). Solid curve represents the experimental data at 623 K (corrected for temperature dependence). The dashed curve (49) portrays the prediction of the homogeneous model.

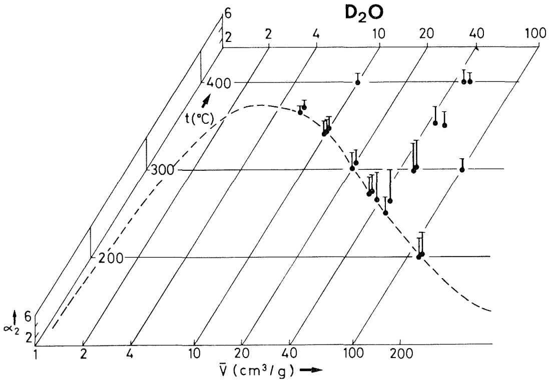

FIG. 19. Density and temperature dependence of the yields and of the localized electrons in D_2O (49). The solid dots represent (ρ, T) points for which experiments were conducted. The vertical lines represent the values of α in arbitrary units. The dashed curve is the liquid–gas CEC. Densities represented in terms of specific volumes $\rho = (\bar{v})^{-1}$.

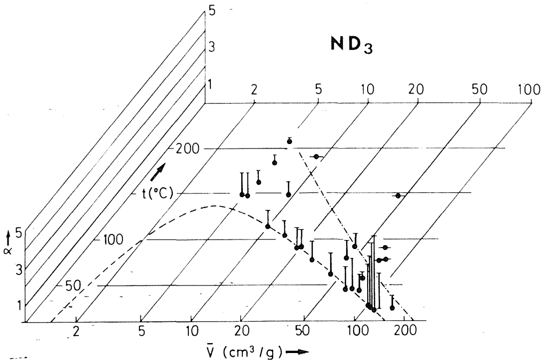

FIG. 20. Density and temperature dependence of the yields of localized electrons in ND_3 (49). Presentation of data identical to those in Fig. 19. Points represented by (—) correspond to ρT values where localized electrons could not be detected. Dashed curve is the liquid–gas CEC. Dotted-dashed curve corresponds to a rough segregation of the ρT plane to two regions where localized states exist and where localized states are thermodynamically unstable.

studied by us, whereupon $\rho_C < 10^{-2}$ g cm^{-3} near the CEC. This observation is again inconsistent with the prediction of the homogeneous model. At high temperatures above the CEC the yield of localized electrons vanishes. In Fig. 20 we have drawn a line in the ρT plane which segregates the range of electron localization from the thermodynamic range where the quasi-free electron state is stable. For these experimental results it is apparent that in supercritical ND_3 ρ_C is determined not only by density but also by the temperature.

TABLE 8. Critical densities for electron localization in polar fluids

	Model calculations		Experimental
	N	ρ_C (g cm^{-3})	ρ_C (g cm^{-3})
H_2O	4	0.044–0.03	$<5\times10^{-3}$
T = 660 K	6	0.07–0.05	
NH_3	4	0.08–0.065	$<10^{-2}$ near CEC
T = 470 K	6	0.14–0.11	~0.1 40°C above CEC

Although the thermodynamic stability criterion used in the homogeneous model involves a temperature dependence originating from an entropy contribution, the experimental results cannot be accounted for in terms of such a model and in particular the low value of ρ_C near the CEC is striking. On the other hand, at high temperatures above the CEC the predictions of the homogeneous model are not too bad; for example, at 40°C above the CEC $\rho_C \simeq 0.1$ g cm^{-3} in agreement with the observation of Olinger *et al.* (47), in accord with the theoretical prediction (Table 8). However, this minor success does not reconcile the serious discrepancies between the experimental observations and the expectations of the homogeneous model.

These discrepancies between the theoretical homogeneous model and the facts of life can be summarized as follows.

(I) The weak dependence of $h\nu_{\max}$ on ρ at low ($\rho < 0.1$ g cm^{-3}) densities is in conflict with the prediction for a sharp drop of $h\nu_{\max}$ in that range. This theoretical result originates from the decrease (at $\rho < 0.1$ g cm^{-3}) of the polaron coupling parameter $\beta = \varepsilon_{op}^{-1} - \varepsilon_s^{-1}$ which determines the long-range polarization potential.

(II) The low values of ρ_C observed for D_2O over the entire ρT range and for ND_3 near the CEC. The high value of ρ_C predicted by the homogeneous model originates from the following three causes. First, a cluster of $N = 4$ solvent molecules does not localize the excess electron. Second, the sharp decrease of β with decreasing density at low ρ results in a decrease of the ground state energy. Third, the entropy contribution resulting from formation of the first coordination layer from the homogeneous gas is crucial in determining the thermodynamic stability of the localized state.

(III) The strong temperature dependence of ρ_C for ND_3 is inconsistent with the prediction that the density alone is the primary thermodynamic variable of state which determines the stability of the localized state. We are forced to conclude that the homogeneous model is inadequate and propose that the role of pre-existing density fluctuations is crucial in the electron localization process in polar fluids.

We propose that in polar supercritical fluids of polar molecules the quasi-free electron is trapped by density fluctuations. These density fluctuations can be envisioned as pre-existing clusters which act as electron traps. Similar ideas for dynamics of electron localization in liquids were recently advanced by Kenney-Wallace and Jonah (10) and by Baxendale and Sharpe (11). We address ourselves to a more general problem; as in our one-component system the fluid density can be continuously varied, we inquire when is the amplitude of density fluctuations sufficiently low (*i.e.* the size of the pre-existing clusters is too small) so that electron localization will not occur.

To determine the probability of electron capture by density fluctuations two cardinal points have to be elucidated.

(*A*) What is the minimal size of a pre-existing cluster to insure electron capture?

(*B*) What is the probability for density fluctuations of appropriate amplitude to satisfy condition *A*?

To provide a semiquantitative answer to point *A* we have carried out (49) calculations of the ground state energy of an electron localized in a cluster which consists of $N = 4$ molecules in the first coordination layer and N_D molecules in the second coordination layer. These calculations were conducted (49) using a modified version of Iguchi's method (50). We find that the localized excess electron is stable in a cluster of water molecules consisting of $N = 4$ and $N_D \simeq 2$, while for a cluster of ammonia molecules energetic stability is insured for $N = 4$ and $N_D \simeq 6$. Next we turned to point *B* and utilized (49) the simple thermodynamic fluctuation theory to evaluate the probability distribution for density fluctuations consisting of $N_T = N + N_D$ molecules. This probability distribution is determined by the mean density, by the isothermal compressibility, by the temperature, and by N_T. Detailed calculations will be presented elsewhere and only some conclusions of this analysis will now be mentioned. As the compressibility is high near the CEC the probability of density fluctuations characterized by a large amplitude is always sufficiently large to insure electron localization both for D_2O and for ND_3 in that region. As $N_T \simeq 10$ for ND_3 and $N_T \simeq 6$ for D_2O we expect that the probability for sufficiently large density fluctuations in the latter case will be large enough over the entire ρT range studied by us. On the other hand, for ND_3 the value of N_T is sufficiently high so that at sufficiently low densities high above the CEC (where the compressibility is low) the probability for the occurrence of large ($N_T \simeq 10$) clusters is low and electron localization will not occur. All these expectations agree with the experimental observations.

We thus conclude that the role of density fluctuations is crucial in determining the energetics and dynamics of electron localization in polar fluids. We have experimentally followed the life story of the electron in the polar fluid on a long (μs) time scale. Thus, the spectroscopic information obtained by us does not pertain, of course, to the initial state of the localized electron trapped in the pre-existing cluster. Following the initial process of electron localization several dynamic processes will be exhibited which will result in further energetic stabilization of the localized state. These will include dielectric relaxation (10, 11) (induced by the field of the localized charge) of the external polar medium. In low density polar fluids ($\rho < 0.1$ g cm^{-3}) this long-range effect may be less important than in normal liquids. More interesting is the possibility of further clustering of polar molecules around the initially formed charged cluster. Such a 'snowball effect' will result in the formation of a trapped electron localized in a large cluster of polar molecules, which is characterized by a high local density. The 'snowball effect' is reminiscent of electrical stabilization of liquid drops in supersaturated vapors.

One of the compelling reasons for the study of excess electron states in fluids is that excess electrons can be used as probes for the study of molecular geometry and molecular dynamics in normal liquids and in subcritical and supercritical fluids. The results reported herein, as well as the recent investigations of the dynamics of electron localization in He gas (39–44) and in normal liquids (9–11, 51, 52), provide the first steps towards that goal.

1. J. JORTNER and N. R. KESTNER (*Editors*). Electrons in fluids. Springer Verlag, Heidelberg. 1973.
2. Proceedings of Colloque Weyl IV. J. Phys. Chem. **75** (1975).
3. H. T. DAVIS and R. G. BROWN. Adv. Chem. Phys. **31**, 392 (1975).
4. J. JORTNER, N. R. KESTNER, S. A. RICE, and M. H. COHEN. J. Chem. Phys. **43**, 2614 (1965).
5. B. E. SPRINGETT, M. H. COHEN, and J. JORTNER. J. Chem. Phys. **48**, 2720 (1968).
6. N. R. KESTNER. J. Phys. Chem. **79**, 2815 (1975).
7. P. W. ANDERSON. Phys. Rev. **102**, 1008 (1958).
8. M. H. COHEN. Can. J. Chem. This issue.
9. J. CHASE and J. HUNT. J. Phys. Chem. **79**, 2835 (1975).
10. G. A. KENNEY-WALLACE and C. D. JONAH. Chem. Phys. Lett. **39**, 596 (1976).
11. J. H. BAXENDALE and P. H. G. SHARPE. Chem. Phys. Lett. **41**, 440 (1976).
12. J. JORTNER. Electronic excitations in molecular crystals. *In* Vacuum ultraviolet radiation physics. *Edited by* E. E. Koch, R. Haensel, and C. Kunz. Pergamon-Vieweg, Braunschweig. 1974. p. 263.
13. G. BALDINI. Phys. Rev. A, **137**, 508 (1965).
14. A. GEDANKEN, B. RAZ, and J. JORTNER. J. Chem. Phys. **58**, 1178 (1973).
15. D. PUDEWILL, F. J. HUMPSEL, V. SAILE, N. SCHWENTNER, M. SKIBOWSKI, and E. E. KOCH. Phys. Status Solidi. In press (1977) and references therein.
16. R. S. KNOX. Theory of excitons. Academic Press, New York. 1963.
17. S. A. RICE and J. JORTNER. *In* Physics and chemistry of the organic solid state. Vol. 3. *Edited by* F. Fox, M. Labes, and A. Weissberger. Interscience Publishers, New York. 1967. Chapt. 4.
18. J. C. PHILLIPS. *In* Solid state physics. Vol. 18. *Edited by* F. Seitz and D. Turnbull. Academic Press, New York. 1966. p. 55.
19. W. KOHN. *In* Solid state physics. Vol. 5. *Edited by* F. Seitz and D. Turnbull. Academic Press, New York. 1957. p. 258.
20. G. BALDINI. Phys. Rev. A, **137**, 508 (1965).
21. G. BALDINI. Jpn. J. Appl. Phys. Suppl. **14**, 613 (1965).
22. A. GOLD and R. S. KNOX. Phys. Rev. **113**, 834 (1959).
23. A. GEDANKEN, B. RAZ, and J. JORTNER. Chem. Phys. Lett. **14**, 172 (1972).
24. A. GEDANKEN, B. RAZ, and J. JORTNER. Chem. Phys. Lett. **14**, 326 (1972).
25. J. F. O'BRIEN and K. J. TEEGARDEN. Phys. Rev. Lett. **17**, 919 (1966).
26. N. SCHWENTNER, M. SKIBOWSKI, and W. STEINMANN. Phys. Rev. B, **8**, 2965 (1973).
27. Z. OPHIR, B. RAZ, and J. JORTNER. Phys. Rev. Lett. **33**, 415 (1974).
28. Z. OPHIR, B. RAZ, J. JORTNER, V. SAILE, N. SCHWENTNER, E. E. KOCH, M. SKIBOWSKI, and W. STEINMANN. J. Chem. Phys. **62**, 650 (1975).

29. D. PUDEWILL, F. J. HUMPSEL, V. SAILE, N. SCHWENTNER, M. SKIBOWSKI, E. E. KOCH, and J. JORTNER. J. Chem. Phys. **65**, 5226 (1976).
30. Z. OPHIR, N. SCHWENTNER, B. RAZ, M. SKIBOWSKI, and J. JORTNER. J. Chem. Phys. **63**, 1072 (1975).
31. (*a*) W. K. TAUCHERT. Ph.D. Thesis, Free University of Berlin, Berlin, W. Germany. 1975. (*b*) W. K. TAUCHERT, H. JUNGBLUT, and W. F. SCHMIDT. Can. J. Chem. This issue.
32. L. CHIA and P. DELAHAY. (*a*) Unpublished. International Conference on Electrons in Fluids, Banff, Canada, Sept. 5–10, 1976. (*b*) J. Electron Spectrosc. In press.
33. S. A. RICE and J. JORTNER. J. Chem. Phys. **44**, 4470 (1966).
34. D. BEAGEHOLE. Phys. Rev. Lett. **15**, 551 (1965).
35. U. ASAF and J. J. STEINBERGER. Phys. Lett. A, **34**, 207 (1971).
36. B. RAZ and J. JORTNER. Proc. R. Soc. London, Ser. A, **317**, 113 (1970).
37. (*a*) I. MESSING. Ph.D. Thesis, Tel-Aviv University, Tel-Aviv, Israel. 1976. (*b*) I. MESSING, B. RAZ, and J. JORTNER. To be published.
38. M. B. ROBIN. Higher excited states of polyatomic molecules. Vol. I. Academic Press, New York. 1974.
39. (*a*) J. L. LEVINE and J. M. SANDERS. Phys. Rev. Lett. **8**, 159 (1962). (*b*) J. L. LEVINE and J. M. SANDERS. Phys. Rev. **154**, 138 (1967).
40. H. R. HARRISON and B. E. SPRINGETT. Chem. Phys. Lett. **10**, 418 (1971); Phys. Lett. **35**, 73 (1971).
41. J. A. JAHNKE and M. SILVER. Chem. Phys. Lett. **19**, 231 (1973).
42. (*a*) T. P. AGGARTER and M. H. COHEN. Phys. Rev. Lett. **25**, 807 (1970); **27**, 129 (1971). (*b*) T. P. AGGARTER. Phys. Rev. A, **5**, 2496 (1972).
43. J. P. HERNANDEZ. Phys. Rev. A, **7**, 1755 (1973).
44. K. W. SCHWARZ. Unpublished. International Conference on Electrons in Fluids, Banff, Canada, Sept. 5–10, 1976.
45. A. GAATHON and J. JORTNER. Electrons in fluids. Springer Verlag, Heidelberg. 1973. p. 429.
46. R. OLINGER, U. SCHINDEWOLF, A. GAATHON, and J. JORTNER. Ber. Bunsenges. Phys. Chem. **75**, 690 (1971).
47. R. OLINGER, S. HAHNE, and U. SCHINDEWOLF. Ber. Bunsenges. Phys. Chem. **76**, 349 (1972).
48. A. GAATHON, G. CZAPSKI, and J. JORTNER. J. Chem. Phys. **58**, 2648 (1973).
49. A. GAATHON. Ph.D. Thesis, The Hebrew University, Jerusalem, Israel. 1974.
50. K. IGUCHI. J. Chem. Phys. **48**, 1735 (1968).
51. P. M. RENTZEPIS, R. JONES, and J. JORTNER. J. Chem. Phys. **59**, 766 (1973).
52. D. HUPPERT, W. S. STURVE, P. M. RENTZEPIS, and J. JORTNER. J. Chem. Phys. **63**, 1205 (1975).
53. W. T. SOMMER. Phys. Rev. Lett. **12**, 271 (1964).
54. J. LEKNER *et al.* Phys. Rev. **156**, 351 (1972).
55. Z. OPHIR. Ph.D. Thesis, Tel-Aviv University, Tel-Aviv, Israel. 1976.

Discussion

L. Kevan: Do you think the "snowball" effect for electron localization should occur in nonpolar liquids doped with polar molecules? In recent experiments on glassy mixtures of alkanes with alcohols we have not yet found evidence for such an effect. And in liquid mixtures I believe Professor Baxendale also does not find such evidence. It may be that the critical experiment has not yet been performed since alcohol forms clusters in alkanes. What is needed is a polar molecule that does not cluster on nonpolar media.

J. Jortner: The proposed "snowball" effect in subcritical and supercritical polar fluids at moderately low densities involves a formation of a localized state by electron attachment to a (sufficiently large) pre-existing cluster, followed by subsequent attachment of polar molecules to that charged cluster. Such effect will not be observed in glasses because of the low diffusion coefficient of the polar molecules. In liquid mixtures of polar and nonpolar molecules at a low concentration of the former such effects can be exhibited. However, the time scale is unknown.

G. A. Kenney-Wallace: Jonah and I have carried out picosecond pulse radiolysis experiments on alcohols diluted in alkanes and, to quote one example, electron solvation in butanol-*n*-hexane (1:5 mol ratio) mixtures definitely appears to be slower than that in pure butanol, by a factor of about 2. The stable spectrum appears within tens of picoseconds, not nanoseconds as might have been expected for a diffusion process; however, even in this concentration range we expect to have large alcohol clusters and so an adequate number of alcohol molecules are already present and available for the solvation sheath. In order to see any "snowball" effects, as Jortner has suggested, we would have to go to much lower concentrations of alcohol.

J. Jortner: Obviously picosecond studies of the systems investigated by you and by Baxendale at low alcohol concentrations are required to settle the point whether 'condensation' of additional polar molecules on a charged cluster occurs.

A. O. Allen: Conductivity studies of dilute (0.01 *M*) methanol in hydrocarbons shows that an equilibrium exists between mobile electrons and methanol-solvated electrons. The evolution of solvation in time is therefore due (at least in part) to passage from smaller to larger clusters through the conductive (unsolvated) state which exists in thermal equilibrium.

J. Jortner: The peaceful coexistence between extended and localized states at thermal equilibrium in methanol–hydrocarbon mixtures bears a close analogy to the recent experiments of Klaus Schwarz on electron drift velocities in He gas where 'slow' and 'fast' electrons were identified.

N. R. Kestner: Whether or not the "snowballing" effect can be observed after the initial cluster is formed (say in Baxendale's experiments) depends on how long range is the effect of the electron on the fluid. If that potential is reasonably short range, the optical spectra may not change significantly after the initial trap is formed especially if the snowballing involves, say, a third or further coordination layer. We now believe that, in fact, the old theoretical models had a potential which was much too long range.

J. Jortner: The "snowball" effect resembles Thompson condensation of charged droplets occurring on a microscopic scale. One has to distinguish carefully between the nature of the potential acting on the localized electron at long times, whose long-range part is affected by density fluctuation, and the interaction of the charged cluster with polar molecules leading to cluster growth. The invariance of the optical spectrum in D_2O in the density range 0.8–0.01 g cm^{-3} reflects the result of a long time experiment where clustering has been already completed.

L. Onsager: Let me argue for the proposition that the "snowball" forms from the outside in. If we regard the trap formation as a process of dielectric relaxation around a delocalized electron, this will proceed at a rate given by the longitudinal relaxation time $\tau_L = \tau_D\varepsilon_\infty/\varepsilon_0$ in the distant part of the fluid (outside the counteracting region of localization), and the equilibrium polarization in the immediate vicinity is established last.

J. Jortner: Your interesting proposal implies that the initial step in electron localization involves the fast response of the polar medium to a large polaron in an extended state and that the long-range polarization field builds up on a time scale which is considerably shorter than the Debye relaxation time. A few years ago Rentzepis, Jones, and myself proposed that the initial step in electron localization in a polar liquid (water) involves the build-up of the long range dipolar polarization field. However, in low density supercritical polar fluids near the liquid–vapor coexistence curve we have to consider the role of pre-existing clusters (originating from density fluctuations), which act as electron traps.